Selective calculation of high-intensity vibrations in molecular resonance Raman spectra

Karin Kiewisch, Johannes Neugebauer,[a] and Markus Reiher
Laboratorium für Physikalische Chemie, ETH Zurich, Wolfgang-Pauli-Strasse 10, 8093 Zurich, Switzerland

(Received 13 September 2008; accepted 14 October 2008; published online 25 November 2008)

We present an intensity-driven approach for the selective calculation of vibrational modes in molecular resonance Raman spectra. The method exploits the ideas of the mode-tracking algorithm [M. Reiher and J. Neugebauer, J. Chem. Phys. **118**, 1634 (2003)] for the calculation of preselected molecular vibrations and of Heller's gradient approximation [Heller *et al.*, J. Phys. Chem. **86**, 1822 (1982)] for the estimation of resonance Raman intensities. The gradient approximation allows us to construct a basis vector for the subspace iteration carried out in the mode-tracking calculation, which corresponds to an artificial collective motion of the molecule that contains the entire intensity in the resonance Raman spectrum. Subsequently, the algorithm generates new basis vectors from which normal mode approximations are obtained. It is then possible to provide estimates for (i) the accuracy of the normal mode approximations and (ii) the intensity of these modes in the final resonance Raman spectrum. This approach is tested for the examples of uracil and a structural motif from the E colicin binding immunity protein Im7, in which a few aromatic amino acids dominate the resonance Raman spectrum at wavelengths larger than 240 nm. © *2008 American Institute of Physics*. [DOI: 10.1063/1.3013351]

I. INTRODUCTION

Vibrational spectroscopic methods such as infrared and Raman spectroscopy are versatile tools to study the structure and properties of molecules. With increasing size of the molecules, however, the interpretation of the spectra is hampered by the large number of close-lying or even overlapping vibrational peaks. Resonance Raman spectroscopy has the advantage that certain peaks in the vibrational spectra are selectively enhanced, so that the resonance conditions act like a filter on the vibrational spectrum.[1] This makes resonance Raman spectroscopy an attractive spectroscopic method even for the investigation of biomolecules,[2,3] e.g., proteins and light-harvesting systems.[4–6]

The application of theoretical approaches to resonance Raman spectra[7–10] has become feasible for larger molecules in recent years due to the development of reliable methods for the calculation of ground-state vibrational modes and excited electronic states.[11–16] Frequency analyses based on density functional theory are very efficient[17] and yield harmonic frequencies that are usually in very good agreement with fundamental frequencies as obtained in experiment,[18,19] so that intricate features in complicated vibrational spectra can be clarified.[20–22] An analysis on the basis of experimental information alone would be much more difficult in many cases, if possible at all. The development of the mode-tracking algorithm,[23–25] which allows the selective calculation of a subset of predefined normal modes, made it possible to restrict the theoretical frequency analyses to subsets of the Hessian eigenvectors, which are of relevance for a particular problem under study. A necessary condition for an efficient application of the mode-tracking algorithm is that at least a rough guess for the normal modes to be optimized can be provided. Various ways to obtain such a guess have been employed.[24,26–33] For a recent review, see Ref. 25.

While it is sometimes known which vibrations will get enhanced under resonance conditions, this may not be true in general for more complicated molecules, e.g., transition metal compounds.[34] In this work, we explore the possibility to use an algorithm based on the mode-tracking principle together with the information on the excited-state gradient in order to directly determine only the *intense* vibrations in a resonance Raman spectrum. The approximate relative intensity of a vibration within Heller's gradient (or short-time) approximation[7] is related to the projection of the excited-state gradient vector onto that normal mode. The method presented in this work uses this gradient vector as a guess vector in a mode-tracking calculation and subsequently focuses on vibrational normal modes with a large overlap with that vector. Of major importance for the efficiency of the method are the criteria according to which the intense modes are chosen and their convergence is assessed. The algorithm applied here is thus very different from, e.g., the approach presented in Ref. 20, in which the intensities were calculated in a modewise way *after* the vibrational frequencies and normal modes had been determined.

Although this algorithm should be of general use, we are in particular aiming at its application for resonance Raman investigations on (models for) proteins, since the structure elucidation of proteins as well as of other biomolecules is an important field of application for experimental resonance Raman spectroscopy.[35,36] By analyzing the amide vibration wavenumbers and intensities,[37–39] the secondary structure of proteins can be probed. If the excitation wavelength is tuned

[a]Author to whom correspondence should be addressed. Electronic mail: johannes.neugebauer@phys.chem.ethz.ch.

to energies at which bands of the aromatic amino acids tryptophan (Trp), tyrosine (Tyr), and phenylalanine (Phe) are selectively enhanced, information about hydrogen bonds and hydrophobicity of the environment and orientation of these chromophores can be obtained.[37,40–43] Resonance Raman spectroscopy is also a valuable method to aid the study of protein folding, as shown, e.g., in the investigation of variants of the E colicin binding immunity protein Im7 and their different conformational states.[44]

In the following, we will first present the underlying theory and details of the algorithm and implementation (Sec. II) before we study the approach for the calculation of resonance Raman intensities of uracil in Sec. III. An application to models of the protein Im7 follows in Sec. IV before we conclude from our results in Sec. V.

II. THEORY

In order to appreciate the algorithmic structure of the intensity-tracking approach, which focuses exclusively on the determination of high-intensity modes, we briefly review the algorithmically related, though conceptually very different mode-tracking protocol, which is solely based on the form of the collective motion provided as a guess.

A. Mode-tracking algorithm

The full details of the original mode-tracking algorithm have been presented in previous work.[23–25] An outline of the main steps is given in the following. In the mode-tracking algorithm, the eigenvalues λ_i of the Hessian matrix are determined by employing a subspace iteration method such as the Lanczos[45] or Davidson[46] method. In each iteration, approximate solutions for a subset of eigenvectors $\mathbf{L}_i$ are obtained. This procedure can be applied to solve for a certain preselected mode (or, when using a block-Davidson method, several preselected modes), where the iterative algorithm will be carried out until the approximations of the selected eigenvectors are converged. Thus the diagonalization of the full mass-weighted Hessian $\mathbf{H}^{\mathrm{mw}}$,

$$(\mathbf{H}^{\mathrm{mw}} - \lambda_i)\mathbf{L}_i = 0, \tag{1}$$

is formally replaced by solving

$$(\mathbf{H}^{\mathrm{mw}} - \lambda_i^{(k)})\mathbf{L}_i^{(k)} = \mathbf{r}_i^{(k)}, \tag{2}$$

where $\mathbf{r}_i^{(k)}$ is the residuum vector for the approximate eigenvector $\mathbf{L}_i^{(k)}$ in iteration k. The elements of the residuum vector have the same unit as the elements of the mass-weighted Hessian and are given in the following in units of hartree/(amu $\times$ bohr^2), where amu is the atomic mass unit ($1.660\,56 \times 10^{-27}$ kg). The exact eigenvectors of the Hessian provide the unitary transformation matrix from mass-weighted Cartesian ($\mathbf{R}^{\mathrm{mw}}$) to mass-weighted normal coordinates ($\mathbf{Q}$) according to

$$\mathbf{Q} = \mathbf{L}\mathbf{R}^{\mathrm{mw}}, \quad \mathbf{R}^{\mathrm{mw}} = \mathbf{L}^{\dagger}\mathbf{Q}. \tag{3}$$

The eigenvectors $\mathbf{L}_i$, i.e., the columns of the matrix $\mathbf{L}$, describe the normal modes of the molecule.

At the beginning of the mode-tracking calculation, an approximation $\mathbf{b}_i$ for each eigenvector to be optimized has to be chosen. These "guess vectors" represent the first basis vectors (bvs) in which the approximate eigenvectors are expanded. In the following step, the vectors $\boldsymbol{\sigma}_i$ are determined,

$$\boldsymbol{\sigma}_i := \mathbf{H}^{\mathrm{mw}}\mathbf{b}_i, \tag{4}$$

which are calculated numerically as directional derivatives of the gradient of the electronic energy with respect to the bvs. The vectors $\boldsymbol{\sigma}_i$ are used for the calculation of the elements of the small Davidson matrix $\tilde{\mathbf{H}}$,

$$\tilde{H}_{ji} = \mathbf{b}_j^T\mathbf{H}^{\mathrm{mw}}\mathbf{b}_i = \mathbf{b}_j^T\boldsymbol{\sigma}_i. \tag{5}$$

By diagonalization of the Davidson matrix, approximate eigenvalues $\lambda_i^{(k)}$ and eigenvectors $\mathbf{L}_i^{(k)}$ of the full Hessian can be constructed. Subsequently the residuum vectors $\mathbf{r}_i^{(k)}$ are calculated for all $\mathbf{L}_i^{(k)}$ according to Eq. (2).

Afterward, the root homing step is carried out, in which those approximate eigenvectors from the full set $\{\mathbf{L}_i^k\}$ are determined, which correspond to the sought-for vibrations and shall thus be further optimized. This is typically done on the basis of the overlap with either the initial guess vector(s) or the approximate eigenvector(s) selected in the previous iteration.

In a subsequent convergence check, it is tested whether the approximate normal modes are already sufficiently accurate. If not, new bvs are constructed according to

$$\mathbf{b}_{n_b^{(k)}+j} = \mathbf{X}\mathbf{r}_i^{(k)}, \tag{6}$$

where $n_b^{(k)}$ is the number of bvs in iteration k, j runs from 1 to the number of approximate eigenvectors selected for further optimization, and $\mathbf{X}$ is a preconditioner. In our previous investigations, it turned out that even without preconditioning, i.e., by formally choosing $\mathbf{X}=\mathbf{1}$, the algorithm can be applied very efficiently (cf. Ref. 24).

B. Intensity tracking

Intensities for vibrational spectra can be calculated reliably within the double harmonic approximation for infrared and nonresonant Raman spectra. Under resonance conditions, the situation is more complicated, but often an estimate of relative intensities is possible on the basis of the gradient of the excited-state potential energy surface.[7] In those cases, the calculation of relative intensities is even simpler (though less generally applicable) than the calculation of off-resonance Raman intensities.[4,47–51]

The mode-tracking algorithm, as described above, aims at finding those eigenvectors of the Hessian which resemble most closely the predefined collective motion. In contrast to that, intensity tracking aims at the determination of all normal modes of considerable intensity *without an intuitive guess for how these vibrations may look like*. We will show in the following that Heller's gradient approximation offers a way for such an intensity-driven approach for the case of resonance Raman spectroscopy since it can selectively provide information about the movement of the atoms in the intense vibrational modes.

The expression for the relative intensities i_j and i_k in the framework of the gradient approximation[7,9] reads

$$\frac{i_j}{i_k} = \left(\frac{V_j^q}{V_k^q}\right)^2, \tag{7}$$

where V_j^q is the derivative of the excited-state energy with respect to dimensionless normal coordinates $\mathbf{q}$ at the ground state minimum structure $q_j=0$,

$$V_j^q = \left(\frac{\partial E_{\mathrm{ex}}}{\partial q_j}\right)_{\mathbf{q}=0}. \tag{8}$$

These dimensionless normal coordinates q_j are related to mass-weighted normal coordinates Q_j by

$$q_j = Q_j\sqrt{\frac{2\pi c\tilde{\nu}_j}{\hbar}}, \tag{9}$$

where c is the speed of light, $\tilde{\nu}_j$ is the wavenumber of the normal mode q_j, and $\hbar$ is Planck's constant.

Relative intensities are given in terms of the mass-weighted normal coordinates Q_j as

$$\frac{i_j}{i_k} = \frac{\tilde{\nu}_k}{\tilde{\nu}_j}\left(\frac{V_j^Q}{V_k^Q}\right)^2, \tag{10}$$

where

$$V_j^Q = \left(\frac{\partial E_{\mathrm{ex}}}{\partial Q_j}\right)_{\mathbf{Q}=0}. \tag{11}$$

The expression for relative intensities contains the wavenumbers and the gradient of the excited-state energy with respect to the mass-weighted normal coordinates. Although wavenumbers and normal modes of the spectrum are unknown before a vibrational calculation, the excited-state gradient with respect to Cartesian coordinates can be calculated analytically with a single calculation with many excited-state electronic structure methods, e.g., configuration interaction with singly substituted determinants,[52] time-dependent density-functional theory (TDDFT),[53–57] the approximate second-order coupled-cluster method dubbed CC2 model,[58] or the complete active space self-consistent field method.[59]

We can write the expression for V_j^Q explicitly in terms of mass-weighted coordinates as

$$V_j^Q = \sum_i \frac{\partial R_i^{\mathrm{mw}}}{\partial Q_j}\left(\frac{\partial E_{\mathrm{ex}}}{\partial R_i^{\mathrm{mw}}}\right)_{\mathbf{R}=0} = \sum_i L_{ij} g_i^{\mathrm{mw}} = \mathbf{L}_j \cdot \mathbf{g}^{\mathrm{mw}}, \tag{12}$$

where we have introduced the mass-weighted gradient vector $\mathbf{g}^{\mathrm{mw}}$,

$$g_i^{\mathrm{mw}} = \left(\frac{\partial E_{\mathrm{ex}}}{\partial R_i^{\mathrm{mw}}}\right)_{\mathbf{R}=0}, \tag{13}$$

and used Eq. (3) to determine

$$\frac{\partial R_i^{\mathrm{mw}}}{\partial Q_j} = L_{ij}. \tag{14}$$

Equation (12) thus shows that the excited-state derivative along a normal coordinate is equal to the corresponding expansion coefficient of the mass-weighted excited-state gradient vector in terms of normal coordinates, i.e., its projection onto the Hessian eigenvector. Since the intensity is proportional to $(V_j^Q)^2$, intense modes will have a larger overlap with the excited-state gradient vector, so that the gradient resembles a particular normal coordinate the more closely the more intense it is. The excited-state gradient is thus a suitable guess vector for the mode tracking of intense modes. Since the present approach tries to select and optimize *all* normal modes that carry a significant percentage of the total intensity, irrespective of the type of motion, the root homing procedure, i.e., the selection of eigenvector approximations for further optimization, has to be adapted in order to choose the most intense modes.

During the intensity-tracking iterations, only approximate normal mode vectors are available at the beginning. An expression for the approximate relative intensity of mode j can be derived from Eqs. (10) and (12),

$$i_{j,\mathrm{rel}} = \frac{1}{\tilde{\nu}_j}(V_j^Q)^2 = \frac{1}{\tilde{\nu}_j}(\mathbf{L}_j \cdot \mathbf{g}^{\mathrm{mw}})^2, \tag{15}$$

where the eigenvectors $\mathbf{L}_j$ and wavenumbers $\tilde{\nu}_j$ have to be replaced by their current approximations.

Modes, which according to Eq. (15) have a high approximate (relative) intensity, are selected for further optimization. There are several possible schemes to implement such a root-homing procedure, of which we have tested (i) the selection of the N most intense modes in each iteration and (ii) the selection of a certain number of modes in such a way that their relative intensities sum up to a certain percentage of the total intensity. The subsequent steps, i.e., convergence check and construction of new bvs, follow the standard mode-tracking procedure. The description of the most intense modes is iteratively improved until they are converged, so that we obtain an approximate resonance Raman spectrum which is accurate with respect to the most intense modes. The gain in efficiency compared to a conventional calculation of the resonance Raman spectrum should thus be the larger the more low-intensity modes are present in the spectrum, since these modes will be automatically discarded in the intensity-tracking calculation.

The qualitative difference between mode-tracking and intensity-tracking calculations is illustrated in Fig. 1. Whereas the primary goal of mode tracking is to determine the exact normal mode and frequency of a *specific* vibration for which an intuitive guess was supplied, the aim of intensity tracking is an iterative refinement of an entire spectrum based on an unspecific guess that corresponds to a hypothetical vibration carrying the entire intensity.

C. Technical details

DFT ground-state structure optimizations and calculations of excitation energies, excited-state gradients, as well as raw-data calculations of energy gradients needed for the intensity-tracking approach were performed with the hybrid functional B3LYP (Refs. 60–63) and the Becke–Perdew (BP86) functional[62,64] employing the TZVP basis sets implemented in TURBOMOLE.[65,66] In case of BP86, we applied the resolution-of-the-identity approximation. Note that only one excited-state gradient calculation at the ground-state equilibrium position is needed for resonance-Raman calculations within Heller's gradient approximation. Mode-tracking and

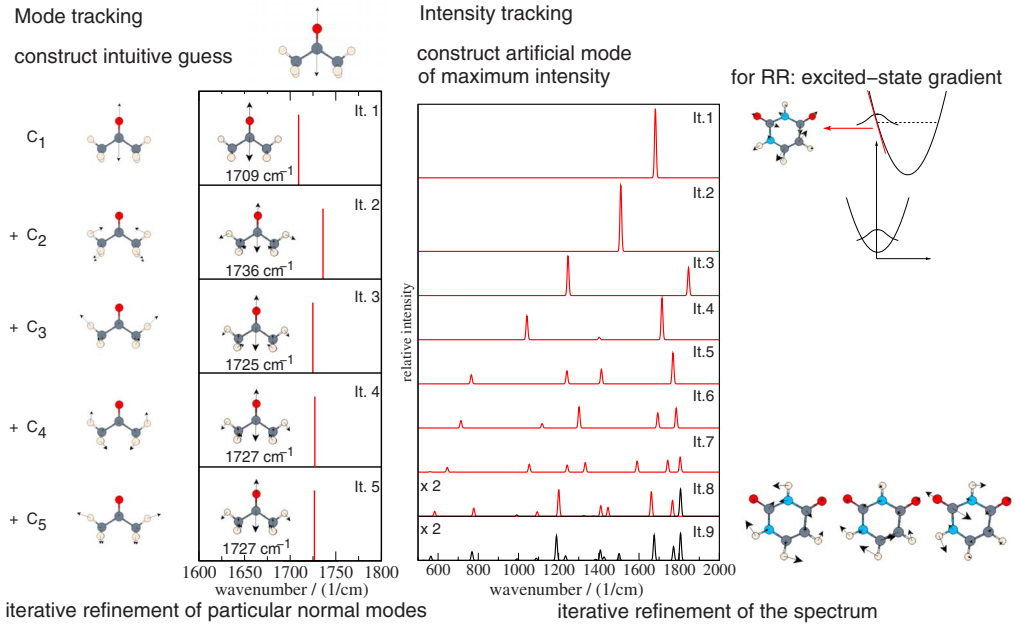

FIG. 1. (Color online) Schematic comparison of mode tracking (left) and intensity tracking (right). In the former case, a guess for a specific normal mode of the molecule under study is created, which is iteratively refined to get the exact normal mode and vibrational frequency. In contrast to this, intensity tracking starts with an unspecific guess for a hypothetical collective motion that contains the entire intensity in the resonance Raman spectrum. A guess for the entire spectrum is then iteratively refined. The intermediate spectra shown on the right are taken from a B3LYP/TZVP resonance Raman calculation on uracil, assuming resonance with the $2^1A'$ state.

intensity-tracking calculations were carried out with a modified version of the program AKIRA.[23] If not specified otherwise, standard AKIRA convergence criteria and an intensity threshold of 80% of the total intensity for root homing were applied (see below). For comparison, excited-state gradients were projected onto normal modes calculated by a complete frequency calculation with the SNF program.[17] These spectra are dubbed "conventional gradient spectra." All resonance Raman spectra are plotted applying a Gaussian broadening with a half width of 10 cm^{-1}.

III. VALIDATION: INTENSITY TRACKING FOR URACIL

In order to validate the intensity-tracking algorithm, we calculate the resonance Raman spectrum for the $2^1A'$ state of uracil, which has been well studied with various theoretical methods.[48,67] Uracil is a planar molecule and, within Heller's gradient approximation, resonance Raman active vibrations must be in that plane (a' symmetry). Our mode-tracking implementation does not explicitly consider the molecular symmetry for the calculations, but allows the creation of an orthogonal subspace against which new basis modes are orthonormalized. The optimized C_s symmetric uracil structure, see Fig. 2, was obtained using B3LYP/TZVP and the gradient of the $2^1A'$ state at 5.25 eV. Since uracil is a planar molecule with 12 atoms, there are $12\times2=24$ degrees of freedom in the xy-plane. Two of them represent translations and one is a rotation, so that there are 21 degrees of freedom for vibrational motion relevant for the current test.

We expect the intensity-tracking algorithm to work best for electronic transitions localized on a small part of a larger molecule with localized vibrational modes since a smaller number of bvs will be needed for their description. The decrease in central processing unit (CPU) time of the intensity-tracking calculation compared to a full seminumerical calculation of the vibrational spectrum[17] is given by the ratio of the number of bvs needed in comparison with the total number of vibrational degrees of freedom of the molecule since for both methods there is a linear correlation between the number of bvs and the CPU time needed. Intermediate intensity calculations and the root-homing procedure produce only a small overhead.

Uracil does not at all fulfill this prerequisite since the molecular orbitals involved in the electronic transition under study are basically delocalized over the entire molecule (see Fig. 2). Therefore, this small molecule represents the most critical test case for the convergence behavior of the intensity-tracking algorithm since the mode construction cannot benefit from intensity selection. This is reflected in the current example by the necessity to include all 21 bvs in order to converge the spectrum if rather strict convergence criteria are applied. The intermediate and final spectra are depicted in Fig. 1. The spectrum in the first iteration contains the intensity of all modes concentrated in one peak, which

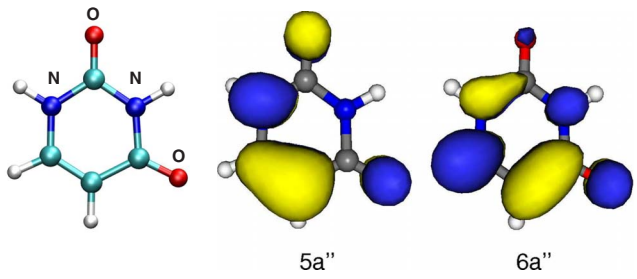

FIG. 2. (Color online) B3LYP/TZVP optimized structure of uracil (C_s symmetry) and molecular orbitals (B3LYP/TZVP) dominating the transition to the $2^1A'$ state of uracil.

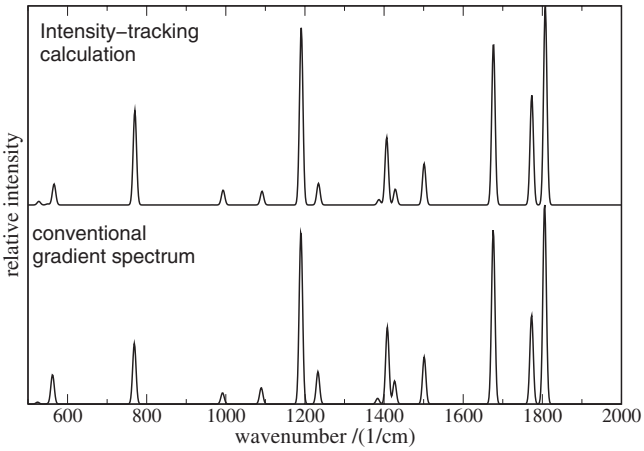

FIG. 3. Comparison of the converged resonance Raman spectrum (B3LYP/TZVP) of uracil from an intensity-tracking calculation (top) and a conventional (reference) gradient spectrum (bottom) assuming resonance with the $2^1A'$ state.

corresponds to the collective motion given by the excited-state gradient vector. Note that its approximate eigenvalue is already quite close to the frequency of the most intense mode in the converged spectrum. In the following iterations, the intensity is distributed to more and better approximations of the normal modes (note that in Fig. 1 only vibrations between 500 and 2000 cm^{-1} are shown). Enlarging the basis leads to a shift in the wavenumbers and appearance of new modes. New approximate normal modes which carry a substantial fraction of the intensity are selected for further optimization in the root-homing step. Such modes may split up in subsequent iterations (cf. Fig. 1, iteration 4 to iteration 5). After a few iterations, the most important features are obtained, i.e., the approximate frequencies of the intense peaks and their relative intensities do not change anymore. For example, the two most intense peaks already appear at approximately correct positions after three iterations. The spectrum in iteration 8 represents already a good approximation to the final spectrum. Several modes that are not converged according to the applied criteria hardly change when compared to the subsequent iteration. This suggests that the applied convergence criteria are too strict. Another important aspect for the convergence behavior of the spectra is the choice of the selected modes and thus the root-homing procedure, which will be analyzed in Sec. IV. In a complete basis, the converged intensity-tracking spectrum and the conventional gradient spectrum are virtually identical, see Fig. 3. The marginal remaining deviations are due to the fact that the numerical differentiations applied in both types of calculations make use of different bvs, so that they are affected by numerical noise in slightly different ways.

IV. RESONANCE RAMAN SPECTRA OF IM7-BASED MODELS

Intensity-tracking is expected to be most valuable in cases of large molecules with a comparatively small number of intense vibrations. In the following, we will show how the iterative refinement of signatures in a resonance Raman spectrum can be optimized if these requirements are fulfilled. As an example, we study models derived from the Im7 protein, that all contain the skatole motif from the Trp residue.

This investigation requires several steps. First, the excited states of the core chromophore, i.e., the skatole moiety of the Trp residue, will be investigated in order to identify possible states in resonance, and its conventional gradient spectra are determined. Second, we will map the excited states for Im7-based models to those of skatole in order to identify the resonant states for UV resonance Raman spectroscopy. After these steps have been carried out, we will determine which convergence criteria are necessary in order to obtain reliable spectral features, and how the convergence behavior can be controlled and steered in such a way that it allows fast access to the characteristic signatures. Finally, we will apply the criteria obtained from these investigations in a model calculation of the resonance Raman spectrum for a large fragment of the Im7 protein.

A. Preparatory calculations: Identification of resonating states

The calculation of resonance Raman spectra in Heller's gradient approximation requires, as a first step, the identification of the excited state responsible for the resonance enhancement. The criteria that can be used for this purpose are the requirements that (i) the resonance condition with the incident light beam is fulfilled for the excited state and that (ii) the transition dipole moment for the corresponding transition is large. For the larger Im7-based models that we are aiming at, TDDFT is the only applicable first-principles method for excited states since it offers a good compromise between accuracy and computational cost, in particular for the valence excited states that are studied in this work. However, it is well known that TDDFT suffers from several problems that lead to an underestimation of certain types of excitation energies (see, e.g., Refs. 68–70 and references therein). The number of low-lying excited states is thus artificially increased in such calculations, and the oscillator strength of intense electronic transitions may be distributed over several close-lying excitations by spurious mixings.[70] This clearly hampers the identification of excited states that are relevant for the resonance Raman spectrum.

Therefore, we chose two models of different sizes for that part of the Im7 protein that contains the Trp fragment and mapped their excited states to those of the bare skatole chromophore. Note that the full Im7 protein also contains three Tyr residues that are important for the total resonance Raman spectrum, which we ignored in our study in order to set up model compounds in which one particular chromophore can be assumed to be responsible for the intensity pattern to be tracked.

In Fig. 4, the optimized structures of skatole as a zeroth-order model for Trp in Im7 (in a C_s symmetric minimum structure) and of the Im7-based models 1 and 2 are shown. For the optimization of the ground-state structures, frequency analyses, excitation energies, and excited-state gradients of skatole and model 1, we employed B3LYP/TZVP, whereas for the larger model 2, BP86 was used for the ground-state structures and frequency analysis for efficiency

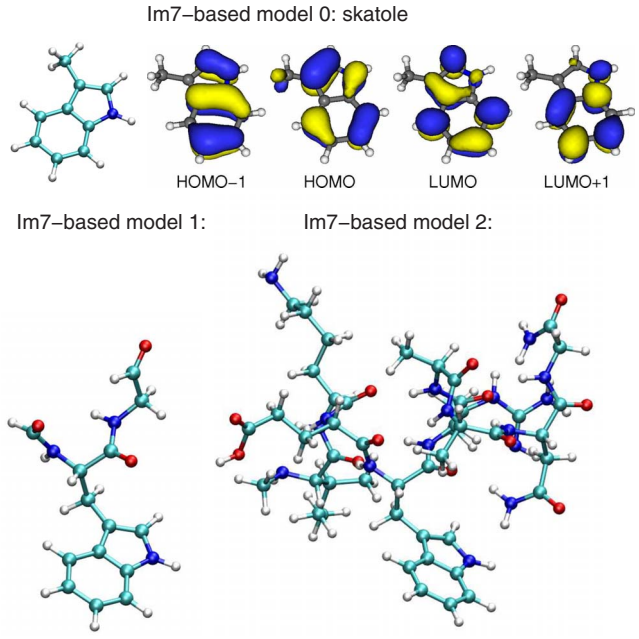

FIG. 4. (Color online) B3LYP/TZVP optimized structures of skatole (C_s) and model 1 as well as the BP86/TZVP optimized structure of model 2. Also shown are the molecular orbitals (B3LYP/TZVP) involved in the lowest electronic excitations of skatole.

reasons. The implications of using different functionals for ground and excited states will be discussed below.

The small Im7-based model 1 comprises 35 atoms and consists of the amino acid Trp, capped by an aldehyde group at the N-terminus and a glycine fragment (instead of the arginine residue) connected to the C-terminus, see Fig. 4. Model 2 consists of the amino acid sequence Ile–Lys–Glu–Trp–Arg–Ala–Ala–Asn–Gly (151 atoms), in which Lys and Arg are included in their neutral form. The structures of both models were fully optimized.

In Table I, excitation energies, transition dipole moments, and dominant orbital transitions are presented. In the wavelength regime between 250 and 280 nm (energy range from 4.4 to 5.0 eV), which we will assume for the excitation wavelength, we obtained two excited states for skatole, which are denoted as L_a (2^1A) and L_b (3^1A). Note that in our DFT study, the order of these two states is reversed in comparison to, e.g., the study on the corresponding states in indole in Ref. 71 and the experimental findings mentioned there. This problem has been discussed in detail for other aromatic compounds before.[72] The 2^1A state is dominated by the HOMO→LUMO orbital transition (HOMO denotes highest occupied molecular orbital and LUMO denotes lowest unoccupied molecular orbital), while a combination of the HOMO−1→LUMO and HOMO→LUMO+1 orbital transitions is dominant for the 3^1A state. Isosurface plots of the orbitals involved are shown in Fig. 4. Since the 2^1A and 3^1A states are only 0.25 eV apart in energy for B3LYP and 0.37 eV for BP86, they can both be expected to contribute to a resonance Raman spectrum with an excitation energy in that range. The experimental excitation energies for both states are somewhat smaller, but similarly close (4.31 and ~4.77 eV,[73] respectively). A detailed theoretical study of the excited states of the underlying indole motif can be found in Ref. 71.

Within Heller's gradient approximation, it is always assumed that only one excited state is in resonance, which is clearly a simplification in the present case. In principle, the approach could also be applied to identify the most important modes for two or more close-lying states. Once these vibrations are identified, more sophisticated treatments taking interference effects into account could be applied subsequently in the restricted set of normal modes. For this pilot study of the intensity-tracking algorithm, however, we will make the approximation that either the L_a or the L_b state alone determine the spectrum.

For model 1, the identification of these states is straight-

TABLE I. Calculated excitation energies, dominant orbital transitions, and corresponding transition dipole moments μ_t for skatole and models 1 and 2. The applied functionals are denoted in parentheses. Where two different functionals are denoted, the first one was used for the ground state structure and frequencies and the second one for excitation energies and the excited-state gradient. Note that the transition mentioned in the first column always refers to the corresponding transition in skatole; H denotes HOMO and L denotes LUMO.

Transition	Molecule	State	Transition	E/eV	μ_t/a.u.
H→L	Skatole (B3LYP)	$2^1A'$	$6a''-7a''$ (89%)	4.62	0.78
	Skatole (BP86)	$2^1A'$	$6a''-7a''$ (88%)	4.20	0.67
	Model 1 (B3LYP)	4^1A	$72a-74a$ (89%)	4.64	0.78
	Model 1 (BP86/B3LYP)	4^1A	$72a-74a$ (86%)	4.58	0.78
	Model 1 (BP86)	8^1A	$72a-74a$ (78%)	4.17	0.64
	Model 2 (BP86/B3LYP)	15^1A	$283a-288a$ (65%)	4.59	0.59
	Model 2 (BP86)	92^1A	$279a-288a$ (46%)	4.26	0.46
H−1→L +H→L+1	Skatole (B3LYP)	$3^1A'$	$5a''-7a''$ (60%) $6a''-8a''$ (37%)	4.87	0.42
	Skatole (BP86)	$3^1A'$	$5a''-7a''$ (55%) $6a''-8a''$ (44%)	4.57	0.25
	Model 1 (B3LYP)	6^1A	$71a-74a$ (61%) $72a-78a$ (25%)	4.87	0.44
	Model 1 (BP86)	12^1A	$71a-74a$ (45%) $72a-77a$ (40%)	4.57	0.28

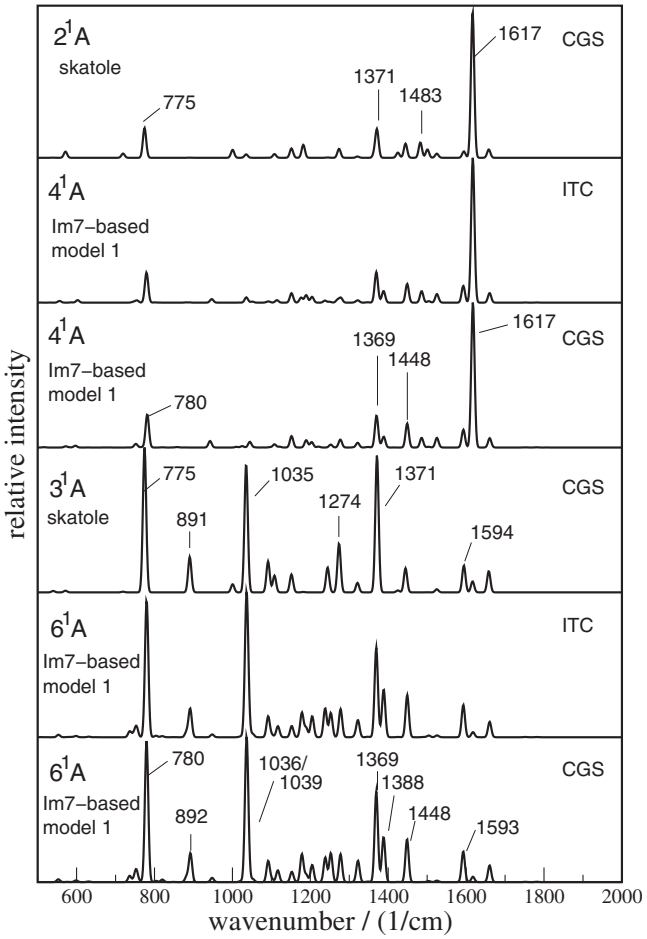

FIG. 5. Resonance Raman spectra of skatole for resonance with the $2^1A'$ or $3^1A'$ state obtained by a conventional gradient calculation using B3LYP/TZVP. Also shown are the spectra for the corresponding states of Im7-based model 1 obtained either in a converged intensity-tracking calculation (ITC) or as conventional gradient spectra (CGS). Wavenumbers of important vibrations are given in units of cm^{-1}.

forward by comparing the excitation energies, transition dipole moments, and orbital transitions involved in the excitations to those of skatole (see Table I). The situation for model 2 is more complicated and not unambiguous due to the problems outlined above for TDDFT calculations on large systems. However, the choice of the resonating states made here can be assessed by comparing the final resonance Raman spectra to those of the smaller structural motifs, which will be done in Sec. IV D.

While the state corresponding to the 2^1A state of skatole was investigated for both models, the excited state corresponding to the 3^1A state of skatole was only examined for model 1 in order to test convergence criteria and root-homing options. As will be shown below, the intensity distribution for this state is distinctly different from that of the 2^1A state, so that the requirements for the intensity-tracking algorithm to converge quickly can be tested on a broader basis.

The B3LYP/TZVP resonance Raman spectrum obtained within Heller's gradient approximation by assuming resonance with the $2^1A'$ state of skatole is shown in Fig. 5. It is dominated by the peak at 1617 cm^{-1}, and two further intense peaks appear at 775 and 1371 cm^{-1}. The corresponding normal modes are visualized in Fig. 6.

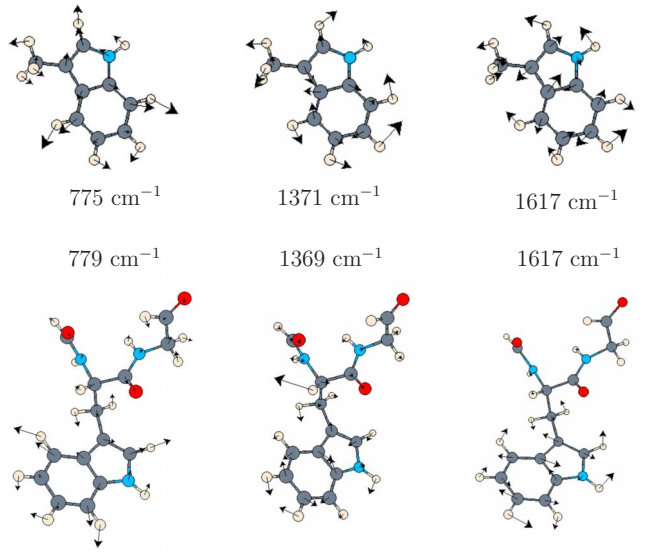

FIG. 6. (Color online) Graphical representation of the intense vibrations (B3LYP/TZVP) in the resonance Raman spectrum of skatole (upper row) and of model 1 (lower row).

In the spectrum obtained from the 3^1A state, the modes at 775, 1035, and 1371 cm^{-1} dominate the spectrum, and several other modes of considerable intensity are present. The enhancement is thus less selective for resonance with this state, and consequently intensity-tracking should be more beneficial for the 2^1A state.

B. Convergence criteria for intensity tracking

In the normal mode-tracking approach, the residuum vector is a measure for the convergence of the sought-after normal mode and its frequency. When studying the convergence of an intensity-tracking calculation, however, two aspects have to be taken into consideration: The first is the selection of reliable criteria for the convergence of the vibrational peaks chosen for optimization in comparison to a conventional calculation. The second concerns the questions of how many and which modes should be selected for the iterative refinement, which also has direct consequences on the overall convergence of the spectrum, since convergence is only tested for the selected modes. This point will be discussed in Sec. IV C.

The goal of this section is to determine reliable convergence criteria, which yield approximate resonance Raman spectra that are in good agreement with a full calculation of the spectrum with the smallest possible number of bvs. For model 1, a complete basis consists of $35\times3-6=99$ bvs. In the following, the convergence is tested in dependence of the threshold value for the maximum absolute component of the residuum vector ($r_{\max}^{\text{thres}}$).

For model 1 of the Im7 protein, we studied resonance Raman spectra calculated for two excited states, 4^1A and 6^1A, which correspond to the $2^1A'$ and $3^1A'$ states of skatole, respectively. Using strict convergence criteria, the intensity-tracking calculation requires a full basis, and the results of the conventional gradient calculations can be reproduced (see Fig. 5) apart from small numerical deviations. We note

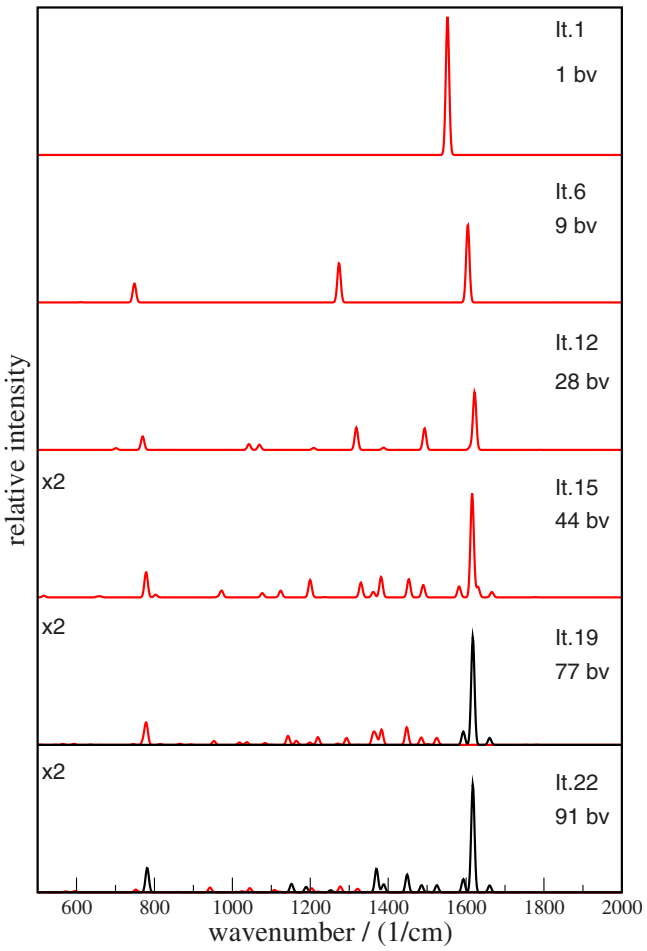

FIG. 7. (Color online) Convergence of the modes during B3LYP/TZVP intensity-tracking iterations (It.) with standard convergence criteria ($r_{\text{thres}}^{\text{max}}$ =0.0005) for the resonance Raman spectrum for the 4^1A state of model 1 (Converged: black; not converged: red). The total number of basis vectors (bv) is given on the right. The relative intensities have a common scale, only the results for iterations 15, 19, and 22 are magnified by a factor of 2.

in passing that the resonance Raman spectrum of the 4^1A state is very similar to the $2^1A'$ spectrum of skatole with respect to the intensity distribution and wavenumbers of the modes. The wavenumbers of the intense modes exhibit only very small shifts, e.g., from 1371 to 1369 cm^{-1}, and the vibrations are mainly localized on the skatole moiety. In Fig. 6, graphical representations of the normal modes are compared to the corresponding skatole modes. The spectrum of model 1 exhibits further modes in the region of 1000–1400 cm^{-1} carrying small percentages of the intensity, but the additional 64 vibrational degrees of freedom compared to skatole do not alter the spectrum significantly.

In Fig. 7, several intermediate spectra during the intensity-tracking iterations with a convergence criterion of $r_{\text{max}}^{\text{thres}}=5\times10^{-4}$ for the third excited state are shown. This leads to a converged spectrum with an almost complete basis of 91 bvs and only minor deviations compared to the conventional gradient spectrum. Although a large percentage of the full set of bvs is required for formal convergence, the most important features of the resonance Raman spectrum are already obtained with good accuracy in iteration 15 with 44 bvs. The convergence criteria are thus obviously too tight if only an approximate spectrum is desired. Additional tests presented in the supplementary material[74] showed that spectra featuring the most significant bands and some additional details can be obtained with an intermediate value for $r_{\text{max}}^{\text{thres}}$ of 3×10^{-3} (46 bv for 4^1A and 55 bv for 5^1A), leading to a reduction in computational effort to 46% and 56%, respectively.

In conclusion, the maximum element of the residuum vector should not be larger than 0.003 in order to get a reasonable approximation to the spectrum. The number of converged modes is in general not well suited to assess the degree of convergence of the overall spectrum.

C. Root homing

In the preceding tests, reasonable spectra required the convergence of a rather large number of modes. This is caused by the fact that too many modes are selected with the root-homing criteria initially applied, especially when the most intense modes are already obtained. The algorithm hence tries to optimize also many lower-intensity modes that may not be relevant for the characteristic features of a spectrum. This results in an almost simultaneous convergence of all selected modes as the basis approaches completeness. A smart root-homing should, on the contrary, lead to a directed convergence of the most intense features of the spectrum and not construct too many new bvs per iteration, so that a smooth development of the spectrum can be expected.

Two possible types of root-homing were tested here: (A) selecting the most intense modes to be optimized so that their cumulative intensity exceeds a threshold percentage of the total intensity I_{thres} or (B) choosing the integer number of N_{sel} most intense modes.

The converged spectra for the third (4^1A) and fifth (6^1A) excited states are depicted in Fig. S2 in the supplementary material.[74] The dependence of the final spectrum on the root-homing option is less pronounced than for the convergence criteria. The tightest threshold considered for each of the three options naturally results in a larger number of bvs and a spectrum which agrees better with the conventional gradient spectrum, since more approximate normal modes are chosen for further optimization. With option (A) and a threshold value of 80% for I_{thres}, a (nearly) complete basis is needed for a converged spectrum. However, even a rather small value of 50% still yields good approximate spectra for this molecule while reducing the number of bvs to 64 bv for 4^1A and 89 bv for 6^1A. Again, it can be seen that the intensity-tracking algorithm works better for the 4^1A spectrum, which contains only a small number of intense bands. With the option to optimize the five most intense modes, i.e., option (B) with $N_{\text{sel}}=5$, the spectrum is well converged for the most important features, and even for $N_{\text{sel}}=3$ the results are only slightly worse.

It should be noted that options (A) and (B) show somewhat complementary features in our tests. Option (B) works well if there is a particular interest in a small number of high-intensity modes, as is the case in the 4^1A spectrum. In the 6^1A spectrum, however, several modes of considerable intensity in the wavenumber range between 1100 and

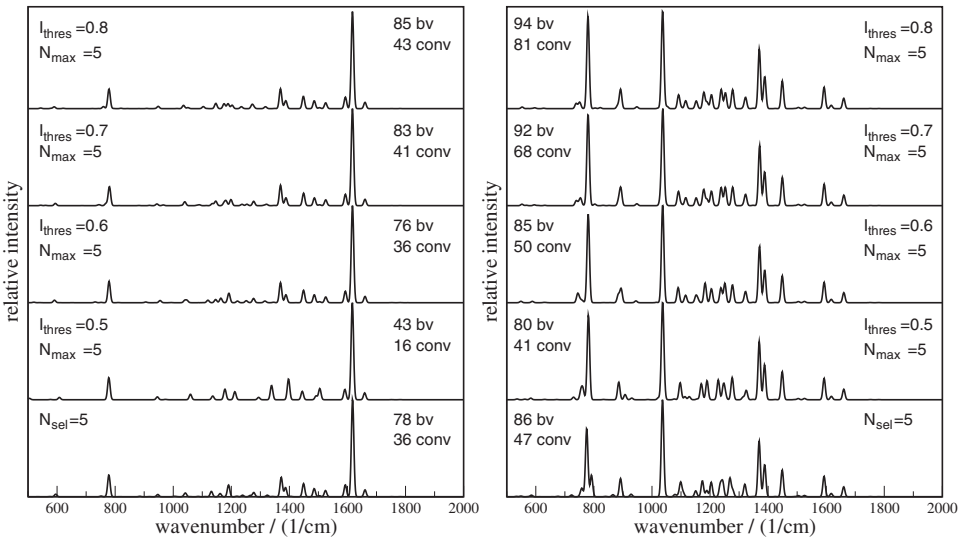

FIG. 8. Converged spectra for the 4^1A (left) and 6^1A (right) state of model 1 for a combination of different root-homing options. A wavenumber selection criterion as mentioned in the main text was applied in all cases. N_{max} indicates for how many of the modes selected by the intensity criterion new basis vectors were created. The total number of basis vectors (bv) and of converged modes (conv) is given for each spectrum.

1350 cm^{-1} are only approximately converged or still missing. Nevertheless, the most dominant bands are clearly converged with option (B), and this option will thus be the preferred one for spectra of larger molecules with only a few significant bands. Option (A) on the other hand guarantees that also those parts of the spectrum are converged in which a considerable part of the total intensity is distributed over a number of modes. However, this often leads to the selection of a large number of approximate modes for further optimization.

In order to avoid these disadvantages in cases where more than just very few modes need to be converged, we also tried a combination of different root-homing criteria. In particular, (i) we applied a wavenumber criterion to all calculations, i.e., only vibrational modes in the range between 500 and 2000 cm^{-1} were chosen for further optimization, and (ii) we selected the modes to be converged according to criterion (A), but only created new bvs for at most N_{max} selected modes in each iteration. The results of these calculations are shown in Fig. 8. It can be seen that in particular for the 4^1A spectrum, a significantly smaller number of bvs is needed, e.g., 43 bvs for the combination $I_{thres}=0.5$, $N_{max}=5$, and the wavenumber test instead of 64 bvs when only the $I_{thres}=0.5$ criterion is applied. For the 6^1A spectrum, the reduction in computational cost is less good, which is most probably related to the fact that a relatively large percentage of the normal modes carry substantial intensity in the spectrum, so that it is very hard to reduce the number of bvs.

D. Intensity tracking for Im7-based model 2

For large models of the Im7 protein, TDDFT yields a multitude of artificially low-lying excited states which mix with the excited states relevant to describe the experimentally observed spectra as can be seen from the data in Table I. These data also show that B3LYP at least partly remedies this problem, since the state corresponding to the 2^1A state of skatole is the 15^1A state of model 2 with B3LYP, whereas it is the 92^1A state in case of BP86, i.e., 77 more low-lying states are found in the BP86 calculation, and it would thus be advantageous to use B3LYP for the entire calculation, as was done for the previous models. However, the pure density functional BP86 leads to an enormous increase in efficiency for large molecules and furthermore gives harmonic vibrational frequencies that are typically in better agreement with experimental fundamental frequencies than B3LYP data.[19] In earlier work,[4] we have successfully tested a hybrid approach in which we calculated the excitation energies and excited-state gradients with B3LYP, whereas BP86 was used for the frequency analysis.

In order to test the effect of this hybrid approach for the class of systems studied here, we compare the resonance Raman spectrum for the 4^1A state of the smaller model 1 obtained with a combination of B3LYP and BP86 to the spectra in which either functional was used consistently in Fig. 9. The main features are identical for all three spectra, whereas the intensity distribution and frequencies of the intense modes change. Comparing the B3LYP/B3LYP spectrum to the BP86/B3LYP spectrum, all intense modes are shifted to lower wavenumbers in the latter calculation while the intensity distribution appears to be roughly the same.

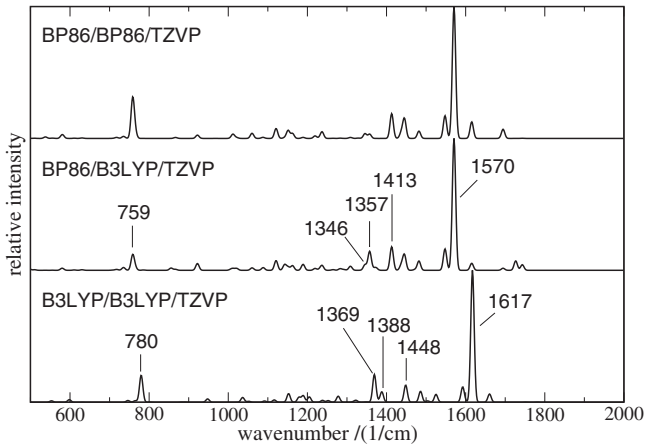

FIG. 9. Resonance Raman spectra of model 1 assuming resonance with the 4^1A state (8^1A in case of BP86/BP86/TZVP) obtained by conventional gradient calculations using different functionals. The first of two given functionals was used for the ground-state structure and frequencies and the second for excitation energies and the excited-state gradient. Wavenumbers of intense vibrations are given in units of cm^{-1}.

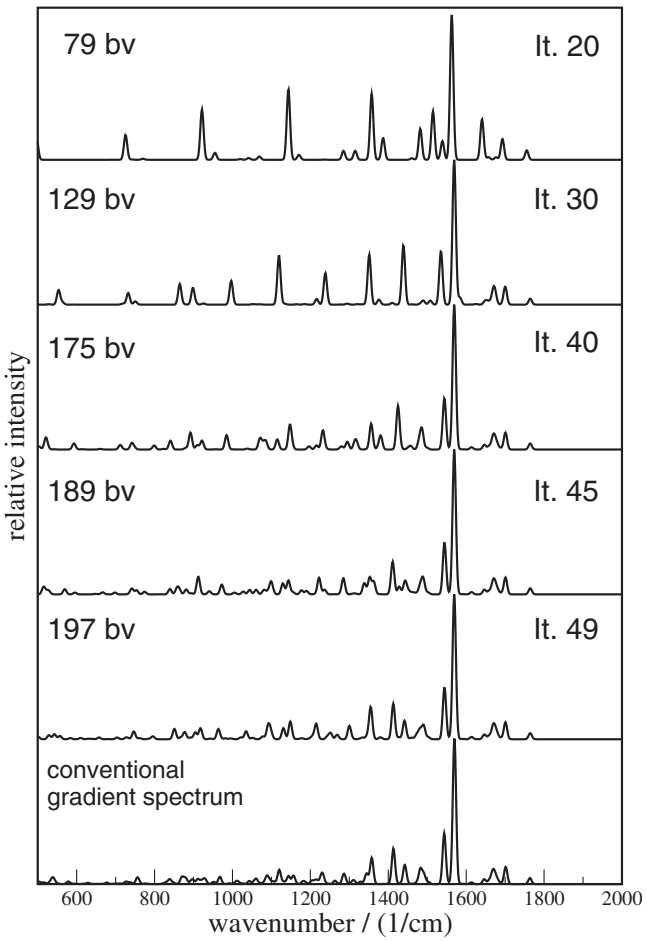

FIG. 10. Convergence of the spectra during BP86/TZVP intensity-tracking iterations (It.) for model 2, starting from the (B3LYP/TZVP) gradient of the 15^1A state. The total number of basis vectors (bv) is given on the left. Lowest panel: conventional (reference) gradient spectrum

Below 1400 cm^{-1}, the intensity pattern seems to be changed. However, a closer inspection reveals that the mode at 1388 cm^{-1} in the B3LYP calculation is shifted to 1346 cm^{-1} in the BP86 calculation, which leads to the slightly different appearance. Further notable differences are the additional intense modes at about 1720 cm^{-1} in the BP86/B3LYP calculation. Deviations in the intensity distribution between the BP86/B3LYP calculation and the pure BP86 calculation can be observed for the modes at 759 cm^{-1}, at about 1350 cm^{-1} and at about 1720 cm^{-1}. Overall, the most intense features of the two spectra are sufficiently consistent, so that the BP86/B3LYP hybrid approach will be used in the following for the large model 2.

With this hybrid approach, we performed intensity-tracking calculations on the excited electronic states of model 2. This model consists of 151 atoms, so that there are 453 degrees of freedom in total, and a complete vibrational basis comprises 447 bvs. We performed an intensity-tracking calculation with root-homing scheme (B) and a selection criterion of $N_{sel}=5$. Additionally, the wavenumber criterion 500 $cm^{-1}<\tilde{\nu}<2000$ cm^{-1} was applied. The approximate spectra for different iterations are shown in Fig. 10. It can clearly be seen that the most intense band at ~1570 cm^{-1} is practically converged already in the first intermediate spectrum shown, which utilizes 79 bvs. In the next spectrum, based on 129 bvs, all features in the range between 1500 and 1800 cm^{-1} with appreciable intensity are virtually converged. Formal convergence is achieved with 197 bvs, and by comparison with the conventional gradient spectrum it can be seen that indeed all the intense bands, which are located between ~1350 and 1800 cm^{-1}, are very well reproduced by the intensity-tracking calculation. Furthermore, the overall impression of the intensity distribution in the lower-wavenumber range is also qualitatively correct. We confirmed that better agreement with the reference spectrum can be obtained, e.g., by applying the hybrid root-homing procedure outlined in the last section, but the selection criterion of $N_{sel}=5$ offers a good compromise between accuracy and efficiency. Only 44% of the full number of bvs are needed to accurately reproduce the intense features in the spectrum, which also means that the CPU time in comparison with a full seminumerical calculation of the vibrational spectrum is reduced to roughly 44%.

V. CONCLUSIONS

In this work, we investigated the possibility to efficiently obtain the characteristic features of a resonance Raman spectrum on the basis of an intensity-driven algorithm. In this way, we can exploit the selectivity that is inherent to experimental resonance Raman spectroscopy also within a theoretical framework. The two following steps are essential for this purpose: (i) the construction of a guess vector for a hypothetical collective motion that contains the entire intensity in the resonance Raman spectrum and (ii) the iterative refinement of approximate normal modes which potentially carry a high intensity. The first step can be addressed by taking advantage of Heller's gradient approximation for relative resonance Raman intensities. For the second part, we developed and tested several selection procedures within an algorithm analogous to the mode-tracking scheme.

It was shown that conventional gradient spectra can be reproduced very well if strict convergence criteria are applied, which is a necessary condition for a successful application of this algorithm. Subsequently, we demonstrated that different root-homing procedures for the selection of modes for further optimization can be used to control the convergence behavior of the calculation. It turned out that root-homing option (B), in which a fixed number of intense modes is chosen in each iteration, gives fast access to the most intense features in the resonance Raman spectrum. In contrast to this, the option in which a threshold for the cumulative intensity is applied (A) allows to quickly determine which wavenumber range is covered by intense vibrations in the spectrum. Option (B) is thus favorable in typical applications of large molecular systems with only a few intense vibrations in the resonance Raman spectrum. This was confirmed in the example of the resonance Raman spectrum of Im7 models, in which the Trp residue shows characteristic peaks. A possible problem with option (A) is that too many new bvs are constructed in each iteration, so that a rather sudden convergence is achieved, which typically requires a comparatively large percentage of the total number of pos-

sible bvs. This problem can be solved by restricting the maximum number of new bvs in order to achieve a smooth convergence behavior.

As far as the efficiency is concerned, which can directly be measured as the ratio of the number of bvs needed for convergence and the full number of vibrational degrees of freedom, it must be noted that the convergence in intensity-tracking calculations is intrinsically more difficult than in typical mode-tracking applications for specific vibrations.[26,27,75] The reasons for this behavior are that intensity-tracking calculations (i) target several vibrations, the exact number of which is unknown at the beginning, (ii) start with an unspecific guess for the type of collective motion, and thus typically require more bvs for correction, and (iii) may partially comprise very unspecific modes that easily couple to other vibrations in the molecule, which affects the convergence behavior. In view of these problems, the methodology outlined here appears quite successful in providing insight into the dominant features of the resonance Raman spectrum of large molecules at reduced cost since the only alternative is a full frequency analysis. Further improvements in the convergence control might be possible by defining different convergence criteria for modes of different intensities, for example, in such a way that tight convergence is only requested for those parts of the spectrum that stand out very sharply due to their high intensity.

We would like to note that even in those cases were Heller's gradient approximation is not reliable the present approach can be of great help since the modes obtained are those with the highest Franck–Condon activity. They will thus also be the most important ones for more sophisticated methods for theoretical resonance Raman spectroscopy, e.g., based on sum-over-states or time-dependent approaches. With modified or additional guess vectors, it should also be possible to address cases in which Herzberg–Teller active modes or several excited states play a role. The latter point will be important for reliable predictions of resonance Raman spectra of Trp-containing systems under experimental conditions due to the two close-lying intense transitions of the skatole motif. Since these modifications of the intensity-tracking scheme may introduce additional vibrations with significant intensity, the guess vectors and the root-homing procedure should be carefully tested for such more sophisticated schemes in order to optimize the convergence behavior.

An open question that should be addressed in future work is how efficient preconditioning schemes can be designed for intensity-tracking calculations, i.e., how the construction of new bvs can be optimized for the search of intense normal modes.

ACKNOWLEDGMENTS

K.K. acknowledges funding by a Doktorandenstipendium of the Fonds der Chemischen Industrie (FCI) and J.N. by a Liebig-Stipendium of the FCI. J.N. would like to thank Professor Marcel Nooijen for stimulating discussions on this topic. This work has been supported by the Swiss National Science Foundation SNF (Project No. 200021-113479).

[1] R. S. Czernuszewicz and T. G. Spiro, in *Inorganic Electronic Structure and Spectroscopy: Methodology*, edited by E. Solomon and A. Lever (Wiley, New Jersey, 1999), Vol. 1, pp. 353–441.
[2] R. Schweitzer-Stenner, J. Raman Spectrosc. **36**, 276 (2005).
[3] C. Herrmann and M. Reiher, Top. Curr. Chem. **268**, 85 (2007).
[4] C. Herrmann, J. Neugebauer, M. Presselt, M. Schmitt, S. Rau, J. Popp, and M. Reiher, J. Phys. Chem. B **111**, 6078 (2007).
[5] A. V. Ruban, P. Horton, and B. Robert, Biochemistry **34**, 2333 (1995).
[6] A. Cua, D. H. Stewart, M. J. Reifler, G. W. Brudvig, and D. F. Bocian, J. Am. Chem. Soc. **122**, 2069 (2000).
[7] E. J. Heller, R. L. Sundberg, and D. Tannor, J. Phys. Chem. **86**, 1822 (1982).
[8] A. B. Myers and R. A. Mathies, in *Biological Applications of Raman Spectroscopy: Resonance Raman Spectra of Polyenes and Aromatics*, edited by T. G. Spiro (Wiley, New York, 1987), Vol. 2, pp. 123–166.
[9] A. B. Myers, Chem. Rev. (Washington, D.C.) **96**, 911 (1996).
[10] A. B. Myers, Acc. Chem. Res. **30**, 519 (1997).
[11] L. Jensen, L. L. Zhao, J. Autschbach, and G. C. Schatz, J. Chem. Phys. **123**, 174110 (2005).
[12] L. L. Zhao, L. Jensen, and G. C. Schatz, J. Am. Chem. Soc. **128**, 2911 (2006).
[13] J. Guthmuller and B. Champagne, J. Chem. Phys. **127**, 164507 (2007).
[14] M.-A. Mroginski, K. Németh, I. Magdó, M. Müller, U. Robben, C. D. Védova, P. Hildebrandt, and F. Mark, J. Phys. Chem. B **104**, 10885 (2000).
[15] T. Petrenko and F. Neese, J. Chem. Phys. **127**, 164319 (2007).
[16] F. Neese, T. Petrenko, D. Ganyuschin, and G. Olbrich, Coord. Chem. Rev. **251**, 288 (2007).
[17] J. Neugebauer, M. Reiher, C. Kind, and B. A. Hess, J. Comput. Chem. **23**, 895 (2002).
[18] W. Koch and M. C. Holthausen, *A Chemist's Guide to Density Functional Theory*, 2nd ed. (Wiley, Weinheim, 2000).
[19] J. Neugebauer and B. A. Hess, J. Chem. Phys. **118**, 7215 (2003).
[20] M. Reiher, J. Neugebauer, and B. A. Hess, Z. Phys. Chem. **217**, 91 (2003).
[21] M. Reiher, G. Brehm, and S. Schneider, J. Phys. Chem. A **108**, 734 (2004).
[22] C. F. Leypold, M. Reiher, G. Brehm, M. O. Schmitt, S. Schneider, P. Matousek, and M. Towrie, Phys. Chem. Chem. Phys. **5**, 1149 (2003).
[23] M. Reiher and J. Neugebauer, J. Chem. Phys. **118**, 1634 (2003).
[24] M. Reiher and J. Neugebauer, Phys. Chem. Chem. Phys. **6**, 4621 (2004).
[25] C. Herrmann, J. Neugebauer, and M. Reiher, New J. Chem. **31**, 818 (2007).
[26] J. Neugebauer and M. Reiher, J. Comput. Chem. **25**, 587 (2004).
[27] J. Neugebauer and M. Reiher, J. Phys. Chem. A **108**, 2053 (2004).
[28] A. L. Kaledin, J. Chem. Phys. **122**, 184106 (2005).
[29] A. L. Kaledin, M. Kaledin, and J. M. Bowman, J. Chem. Theory Comput. **2**, 166 (2006).
[30] M. Reiher and J. Neugebauer, J. Chem. Phys. **123**, 117101 (2005).
[31] T. B. Adler, N. Borho, M. Reiher, and M. A. Suhm, Angew. Chem., Int. Ed. **45**, 3440 (2006); Angew. Chem. **118**, 3518 (2006).
[32] C. Herrmann and M. Reiher, Surf. Sci. **600**, 1891 (2006).
[33] C. Herrmann, K. Ruud, and M. Reiher, ChemPhysChem **7**, 2189 (2006).
[34] T. Petrenko, K. Ray, K. E. Wieghardt, and F. Neese, J. Am. Chem. Soc. **128**, 4422 (2006).
[35] M. A. Mroginski, D. H. Murgida, and P. Hildebrandt, Acc. Chem. Res. **40**, 258 (2007).
[36] F. Sieber and P. Hildebrandt, *Vibrational Spectroscopy in Life Science* (Wiley, Weinheim, 2007).
[37] J. C. Austin, T. Jordan, and T. G. Spiro, Adv. Spectrosc. **20**, 55 (1993).
[38] P. Huang and E. A. Carter, J. Chem. Phys. **125**, 084102 (2006).
[39] R. A. Copeland and T. G. Spiro, J. Am. Chem. Soc. **108**, 1281 (1986).
[40] K. Asakawa, S. Masuda, and H. Takeuchi, J. Raman Spectrosc. **37**, 255 (2006).
[41] R. G. Efremov, A. V. Feofanov, and I. R. Nabiev, J. Raman Spectrosc. **23**, 69 (1992).
[42] P. G. Hildebrandt, R. A. Copeland, and T. G. Spiro, Biochemistry **27**, 5426 (1988).
[43] Z. Chi and S. A. Asher, J. Phys. Chem. B **102**, 9595 (1998).
[44] I. R. Rodriguez-Mendieta, G. R. Spence, C. Gell, S. E. Radford, and D. A. Smith, Biochemistry **44**, 3306 (2005).
[45] C. Lanczos, J. Res. Natl. Bur. Stand. **45**, 255 (1950).
[46] E. R. Davidson, J. Comput. Phys. **17**, 87 (1975).
[47] A. A. Jarzecki and T. G. Spiro, J. Raman Spectrosc. **32**, 599 (2001).

[48] J. Neugebauer and B. A. Hess, J. Chem. Phys. **120**, 11564 (2004).
[49] J. Neugebauer, E. J. Baerends, E. V. Efremov, F. Ariese, and C. Gooijer, J. Phys. Chem. A **109**, 2100 (2005).
[50] J. Guthmuller and B. Champagne, J. Phys. Chem. A **112**, 3215 (2008).
[51] J. Guthmuller and B. Champagne, ChemPhysChem **9**, 1667 (2008).
[52] J. B. Foresman, M. Head-Gordon, and J. A. Pople, J. Phys. Chem. **96**, 135 (1992).
[53] C. Van Caillie and R. D. Amos, Chem. Phys. Lett. **308**, 249 (1999).
[54] C. Van Caillie and R. D. Amos, Chem. Phys. Lett. **317**, 159 (2000).
[55] F. Furche and R. Ahlrichs, J. Chem. Phys. **117**, 7433 (2002).
[56] J. Hutter, J. Chem. Phys. **118**, 3928 (2003).
[57] F. Furche and R. Ahlrichs, J. Chem. Phys. **117**, 7433 (2002).
[58] A. Köhn and C. Hättig, J. Chem. Phys. **119**, 5021 (2003).
[59] T. Busch, A. D. Esposti, and H.-J. Werner, J. Chem. Phys. **94**, 6708 (1991).
[60] A. D. Becke, J. Chem. Phys. **98**, 5648 (1993).
[61] P. J. Stephens, F. J. Devlin, C. F. Chabalowski, and M. J. Frisch, J. Phys. Chem. **98**, 11623 (1994).
[62] A. D. Becke, Phys. Rev. A **38**, 3098 (1988).
[63] C. Lee, W. Yang, and R. G. Parr, Phys. Rev. B **37**, 785 (1988).
[64] J. P. Perdew, Phys. Rev. B **33**, 8822 (1986).
[65] R. Ahlrichs, M. Bär, M. Häser, H. Horn, and C. Kölmel, Chem. Phys. Lett. **162**, 165 (1989).
[66] TURBOMOLE 5.7, http://www.cosmologic.de
[67] W. L. Peticolas and T. Rush III, J. Comput. Chem. **16**, 1261 (1995).
[68] J. Neugebauer, M. J. Louwerse, E. J. Baerends, and T. A. Wesolowski, J. Chem. Phys. **122**, 094115 (2005).
[69] A. Dreuw and M. Head-Gordon, Chem. Rev. (Washington, D.C.) **105**, 4009 (2005).
[70] J. Neugebauer, O. Gritsenko, and E. J. Baerends, J. Chem. Phys. **124**, 214102 (2006).
[71] L. Serrano-Andrés and B. Roos, J. Am. Chem. Soc. **118**, 185 (1996).
[72] S. Grimme and M. Parac, ChemPhysChem **4**, 292 (2003).
[73] P. Ilich, Can. J. Spectrosc. **32**, 19 (1986).
[74] See EPAPS Document No. E-JCPSA6-129-005843 for additional figures concerning convergence criteria and roothoming options. For more information on EPAPS, see http://www.aip.org/pubservs/epaps.html.
[75] C. Herrmann, J. Neugebauer, and M. Reiher, J. Comput. Chem. **29**, 2460 (2008).